Trans. JWRI, Vol. 25(1996), No.2

Mathematical Modeling of Fusion and Solidification in Laser Welding and Evaluation of Hot Cracking Susceptibility

Akira Matsunawa, Masami Mizutani and Seiji Katayama

Joining and Welding Research Institute, Osaka University

Abstract

It is acknowledged that a pulsed laser spot weld is subjected to rapid solidification and fast cooling rates. It is particularly difficult but important to determine various solidification parameters in terms of development of novel microstructure, prevention of welding defects and improvement in mechanical properties. Therefore, in this study, a heat-conduction and solidification model considering the effect of latent heat was developed to provide a reasonably good knowledge of rapid melting and solidification behaviour in such a spot weld. It was confirmed that the latent heat would greatly affect thermal histories during solidification and growth rates of cellular dendrite tips in solidifying weldpool. The model could be utilized to reduce cracking in a laser spot welding of crack susceptible alloys by giving a proper thermal cycle during solidification. The effect of predicted thermal history was verified by experiments and the validity of model was confirmed in conduction mode fusion welding.

1. Introduction

Laser welding at small heat input, especially pulsed laser welding, can produce narrow melted and heat-affected zones, leading to improvement in mechanical and chemical properties of most processed parts. However, it has been revealed that solidification cracks are likely to occur in laser spot welds of some aluminium alloys and fully austenitic stainless steels[1,2]. It is also known in normal welding that the mechanical properties, po-rosity formation tendency and solidification crack susceptibility of a weld fusion zone are frequently affected by growth rate, and con-sequent mushy zone length, microstructure, microsegregation, phases formed, etc. Such microstructure, microsegregation and cracking tendency are correlated to solidification pa-rameters and factors such as cooling rate, solidification rate and temperature gradient as well as the chemical compositions and partition coefficients of alloying elements[3,4]. It is, therefore, important to know the melting and solidification phenomena, cooling rates, growth rates of dendrite tips, mushy zone regions and so on in terms of the interpretation of improved mechanical properties and the formation and prevention of welding defects. However, it is extremely difficult to directly measure the above phenomena and factors because of small heat affected zones and rapid changes in temperature and solidification rate in laser spot welds.

Transactions of JWRI is published by Joining and Welding Research Institute of Osaka University, Ibaraki, Osaka567, Japan.

Therefore, it would be useful and instructive to estimate the welding phe-nomena, solidification parameters and factors and their effects on microsegregation, cracking susceptibility, etc. by a mathematical model.

In this study, therefore, for the conduction mode laser spot welds in pure metals and alloys, a heat-conduction and solidification model considering the effect of latent heat was aimed to develop and numerically analyze with the objective of obtaining a fundamental knowledge of rapid melting and solidification, thermal histories, growth rates of cellular dendrite tips, variation in solid fraction, mushy zone region, etc. Especially, the effect of the latent heat release was examined on various solidification phenomenon and parameters of aluminium alloys. Moreover, the developed heat-conduction and solidification model was used to obtain a good guiding principle in reducing cracks in commercially available aluminum alloy as well as to predict melting and solidification behaviour of a molten puddle.

2. Mathematical Model of Fusion and Solidification for Conduction Mode Spot Welding

A heat-conduction and solidification model in conduction mode laser spot welding can be formulated under the assumption of axial symmetry, i.e., two dimensional heat conduction in respect to r- and z-axes as depicted in **Fig. 1**. Here, it is assumed that laser energy is absorbed on the flat surface of a semi-infinite plate. The model is applicable to any symmetrical heat source and temporal pulse output power shape. In this work, however, a Gaussian distribution of laser power intensity was used on the basis of measured result of a laser beam through GI fiber. Heat generated on the surface is transferred by heat conduction, and the effect of convection was considered by adopting a higher effective value of thermal diffusivity in liquid phase, if necessary. The surrounding surface boundaries are assumed to be adiabatic.

The differential equation of thermal conduction is written as the following equation (1) if the thermal constants are independent of temperature;

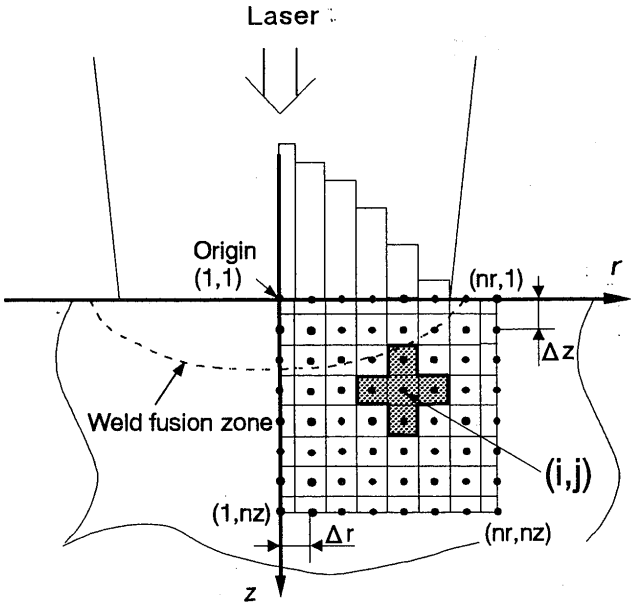

Fig. 1 Schematic representation of mathematical model of fusion and solidification in laser spot welding

$$\frac{\partial T}{\partial t} = \alpha\left(\frac{\partial^2 T}{\partial r^2} + \frac{1}{r}\cdot\frac{\partial T}{\partial r} + \frac{\partial^2 T}{\partial z^2}\right) + \frac{q}{\rho c} \qquad (1)$$

where, $\alpha \equiv \lambda / \rho c$ is thermal diffusivity (m^2/s), and r : the radial distance (m), ρ : density (kg/m^3), c : specific heat (J/(kgK)), T : temperature (K), t: time (s), λ : heat conductivity (W/(Km)), q : heat source term (W/m^3) corresponding to the absorbed laser energy and/or the latent heat of fusion and solidification.

The model was numerically analyzed by the finite difference method. The temperature of the node (i,j) during solidification, for example, is expressed as follows [5]:

$$\begin{aligned} T(\mathrm{i,j})t+\Delta t = {} & \{\alpha\cdot\Delta t\cdot(2r-\Delta r)/(2r\,\Delta r2)\}\cdot \\ & (T(\mathrm{i\text{-}1,j})t - T(\mathrm{i,j})t) \\ & +\{\alpha\cdot\Delta t\cdot(2r+\Delta r)/(2r\,\Delta r2)\}\cdot \\ & (T(\mathrm{i+1,j})t - T(\mathrm{i,j})t) \\ & +\{\alpha\cdot\Delta t/(\Delta z2)\}\cdot(T(\mathrm{i,j\text{-}1})t - \\ & T(\mathrm{i,j})t) \\ & +\{\alpha\cdot\Delta t/(\Delta z2)\}\cdot(T(\mathrm{i,j+1})t - \\ & T(\mathrm{i,j})t) \\ & +L\cdot\Delta fs/c \qquad (2) \end{aligned}$$

where T^t and $T^{t+\Delta t}$: the temperatures at the times t and $t+\Delta t$, respectively; f_s: solid fraction; and L: latent heat.

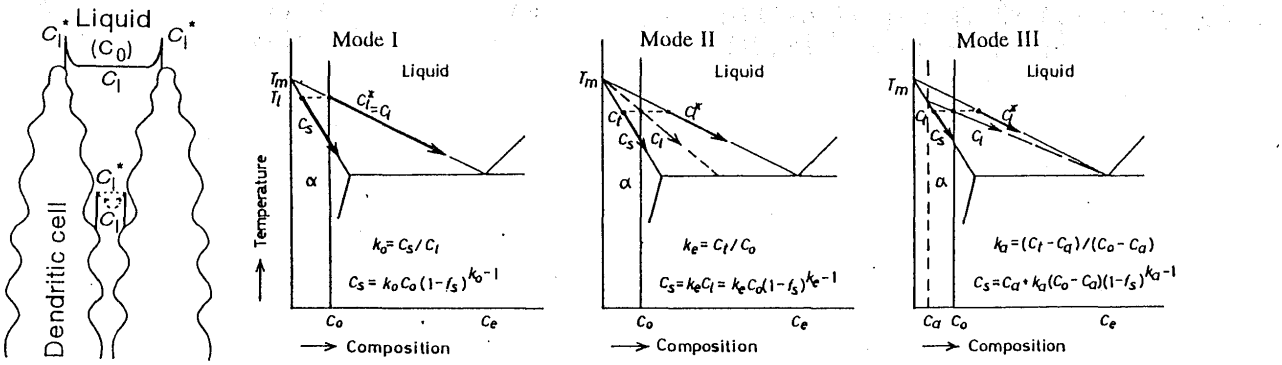

Fig. 2 Schematic cellular dendrite during growth showing solute build–up at boundary, and phase diagrams for three modes of compositional variation, indicating relationship of solute concentrations at solid/liquid interface and in liquid along final boundary

The effect of latent heats of fusion and evaporation were considered by the temperature recovery method[5]. Namely, when the temperature during heating rises above the melting or the evaporation temperature, the former is recovered down to the latter until $f_s = \Sigma \triangle f_s = 1$ by using the the following relation (3):

$$\triangle f_s = c \ \triangle T \ / \ L \qquad (3)$$

where $\triangle T$ is the degree of overheating or undercooling.

On the other hand, during cooling, when the calculated temperature drops below the solidification temperature in the case of a pure metal, it is recovered up to the constant solidification temperature by the equation (3). In the case of an alloy, when the temperature drops below the liquidus $T_l(f_s^t)$, the fraction solid increase $\triangle f_s$ is calculated by the following equation (4), and the temperature is recovered from T_{L0} to $T_l(f_s^t)$

$$\triangle f_s = c \ (T_l(f_s^t) - T_{L0}) \ / \ L \qquad (4)$$

where T_{L0} is the temperature after a time step calculated by assuming $L=0$. While T_l is determined by the liquidus temperature as a function of f_s according to the microsegregation theory. For example, T_l is often expressed in the Scheil's equations (5,6) as follows:

$$T_l = T_f - \left(T_f - T_L\right)\left(1 - f_s\right)^{k_0 - 1}$$
$$for \quad T_E < T_l \quad T_L \qquad (5)$$

$$T_l = T_E$$
$$for \quad 1 - \left\{\left(T_f - T_E\right) / \left(T_f - T_L\right)\right\}^{1/\left(k_0 - 1\right)} \leq f_s \leq 1 \qquad (6)$$

where k_0 is the partition coefficient of alloying element.

The Scheil's equation can not describe the solidification behaviour and microsegregation of alloys under all conditions since it considers neither the diffusion in the solid nor the growth-rate-dependence of partition coefficient at the solid/liquid interface. In spot welds subjected to laser irradiation of millisecond order, the influence of the diffusion in the solid on micro-segregation is negligibly small, but the effects of the undercooling and distribution coefficient should be noticeable. Therefore, in the case of rapid solidification, the undercooling and partition coefficient of solid/liquid interface should be considered to depend upon solidification rate and alloy system[4-16].

The authors[15,16] proposed that the liquidus temperatures for calculations must be determined on the basis of the respective solidification modes describing different compositional changes of solid and liquid in the phase diagrams, as shown in **Fig. 2**. Mode I corresponds to the solidification behaviour according to the Scheil's equation. The distribution coefficient k_0 used was mostly approximated to be a constant for simplicity, but occasionally the partition coefficient and liquidus lines were expressed as fifth-order

Table 1 Nomenclature of symbols, units and constants used in calculation

Symbol (Unit)	Meaning	Constants used
E_0 (J/p)	Laser energy per pulse	15 [17.3, 24.7]**
τ_p (ms)	Pulse duration	5 [5.1, 19.8]**
D_B (mm)	Beam diameter*	1.48 [1.06]**
A (%)	Absorptivity	25 [23]**
T_0 (K)	Initial temperature	293
C_p (J/(Km3))	Specific heat	2.5 x 10^6
L (J/kg)	Latent heat	3.6 x 10^5
Δh_f (J/m^3)	Latent heat of fusion per unit volume	9 x 10^8
α_s (m^2/s)	Thermal diffusivity in solid	7 x 10^{-5}
α_L (m^2/s)	Thermal diffusivity in liquid	7 x 10^{-5}
Δt (s)	Time step	5 x 10^{-8} [2 x 10^{-7}]**
Δz, Δr (m)	Mesh size	5 x 10^{-6} [1 x 10^{-5}]**

* Gaussian distribution of laser power intensity
** Values in [ ] were used for calculation of pulse shaping effect

polynominal as a function of temperature and composition, respectively, for further detailed prediction of microsegregation. In Modes Ⅱ and Ⅲ, the undercooling is considered for rapid solidification. In Mode Ⅱ, the effective partition coefficient k_e is utilized instead of k_0, and consequently the compositions of solid and liquid at the interface of a growing dendrite vary with the solidus line and liquidus line, respectively. In Mode Ⅲ, the duplicate diagram is proposed to satisfactorily explain the effective solidification with the solute-enriched thin layer and to predict microsegregation and temperature distribution. That is to say, the compositions of the solid and liquid at their interface are considered to change with the solidus and liquidus lines, respectively. Also it is significantly taken into consideration that the liquid composition at the final cellular dendritic boundary changes with the tentative liquidus line from the initial average composition (under the undercooling condition due to rapid solidification) to the eutectic point. It may be actual that the liquid composition at the solid/liquid interface of a cellular dendrite should approach the original liquidus line in earlier stages of solidification than the path of Mode Ⅲ, supposing that the thickening rate of dendrite cell trunks is not so high but on the other hand the solute diffusion in the liquid boundary is fast enough.

In this work, the equation was first solved by the recovery method[5] according to the Scheil's equation. Consequently the solidification rates were obtained. On the basis of such solidification rates, the temperature and the liquid and solid compositions of dendrite tips were estimated by using KGT model and Aziz equations. If the degree of undercooling is considerably great, the phase diagram expressed as Mode Ⅲ was deduced, and the calculation of the model was again carried out according to the relationship of Mode Ⅲ. Nomenclature of symbols and constants used in the calculation are tabulated in **Table 1**.

Fig. 2 Schematic cellular dendrite during growth showing solute build-up at boundary, and phase diagrams for three modes of compositional variation, indicating relationship of solute concentrations at solid/liquid interface and in liquid along final boundary

3. Experimental Verification of Model and Discussion

3.1 Material used

The material used was mainly A5083-O aluminium alloy plate of 5mm thickness. The chemical compositions were 4.6%Mg, 0.08%Si, 0.19%Fe, 0.05%Cu, 0.63% Mn and 0.1% Cr. The plate was polished by No. 400 Emery paper and cleansed with Acetone prior to welding. The surface and cross section of a laser spot weld were observed to know the extent of cracking.

3.2 Spot welding with pulsed YAG laser

Spot welding was performed with a pulsed YAG laser in Ar gas atmosphere under various conditions. The laser apparatus used can control the temporal pulse shape of output power within 20ms period[1,2]. A laser beam was delivered through GI fiber of 700 μ m in diameter, and was focused by a quartz lens of 150mm focal length.

The beam analyzer (Big Sky Software Corporation) showed the Gaussian intensity distribution, and it also indicated that the spot size of the laser beam was of about 0.7mm in diameter at the focal point.

3.3 Effect of latent heat on melting and solidification behaviour and solidification parameters in laser spot weld fusion zone

To confirm the effect of latent heat on temperature histories in the weld fusion zone, calculations were first preformed with and without consideration of latent heat during melting and solidification under the conditions that Al-5%Mg alloy plate was exposed to a pulsed laser beam of a Gaussian distribution at low power density during 5ms period. As a result, the temperature histories are indicated in **Fig. 3** at different depths from the surface up to 0.5mm on the central axis of spot weld fusion zone. These thermal cycles are very short. It is understood that, in the case of latent heat considered, the thermal histories at any depths experience slightly lower temperatures due to the latent heat of fusion after the surface melting is initiated, whilst cooling is noticeably delayed owing to the latent heat release after the solidification occurs at the solid/liquid interface along the fusion boundary of the weld pool. Such delay is more remarkable closer to the surface. However, all cooling curves are approaching so closely below 500K that the influence of latent heat becomes negligibly small only 5ms after the laser termination.

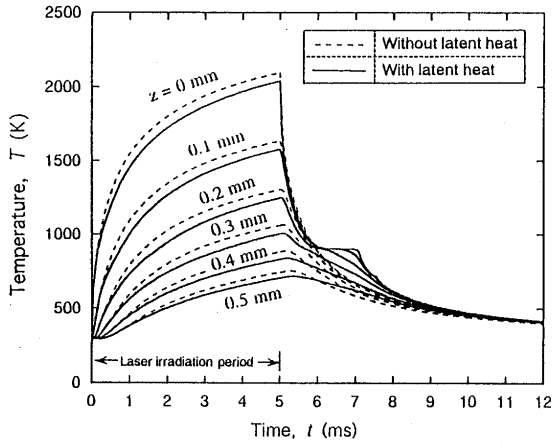

Fig. 3 Calculated temperature histories at different depths of 0 to 0.5mm on central axis of spot weld fusion zone of Al–5%Mg exposed to 5 ms rectangular pulse shape of laser beam.

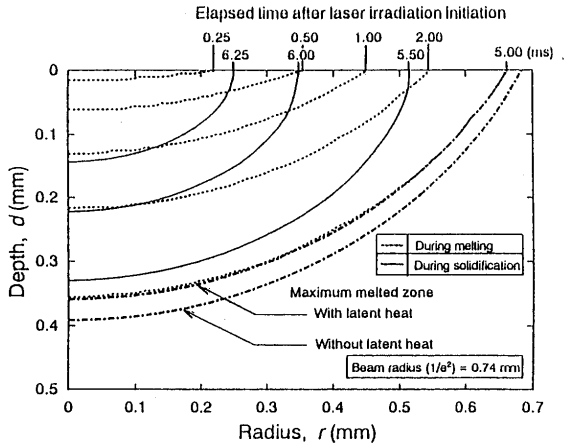

Fig. 4 Variation in isothermal line (corresponding to molten pool geometry) during spot welding, and comparison of resultant fusion zone shapes obtained by using models with and without consideration of latent heat

Figure 4 shows temporal change in the isothermal lines of the melting temperature of Al-5%Mg alloy, signifying the behaviour of rapid melting and solidification of a molten pool. It is apparent that the geometries of molten pool during melting and solidification are different. The molten puddle grows larger

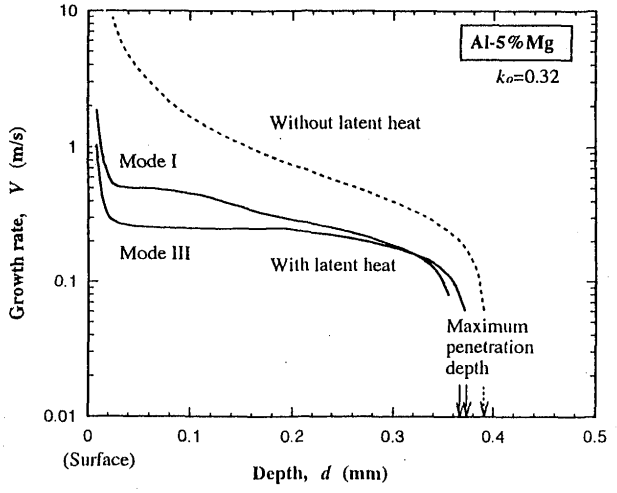

Fig. 5 Growth rates of cellular dendrite tips as function of depth in spot welding of Al–5%Mg alloy, showing effect of latent heat release and influence of solidification microsegregation modes

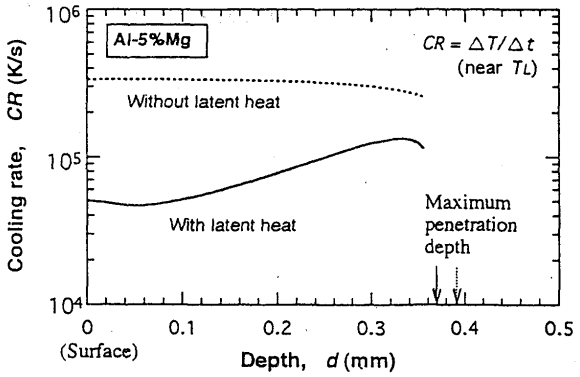

Fig. 6 Calculated cooling rates during welding of Al–5%Mg, showing effect of latent heat evolution

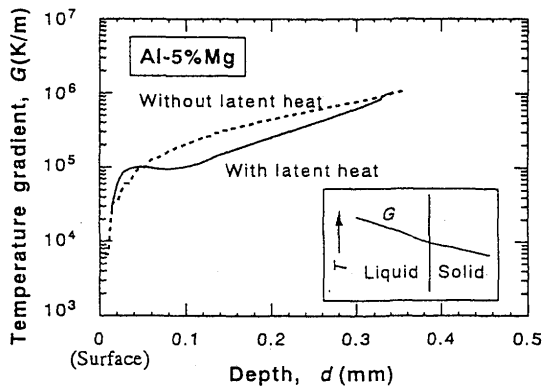

Fig. 7 Temperature gradients at solid : liquid interface calculated by using models with and without considering latent heat

in the relatively flat geometry from the surface owing to distributed heat source during melting. On the other hand, during solidification, it becomes smaller in the half-round shape due to the crystallization and growth from the periphery of the melted zone and easier thermal conduction in the radial direction. It grows only slightly (about 5 μ m) larger near the bottom just after the laser termination. It is also found that the final penetration depth becomes shallow to a small extent (about 30 μ m) on account of the latent heat of fusion.

Subsequently, the growth rates of cellular dendrite tips were estimated by dividing the distances between respective nodes (mesh sizes) by the time differences of their solidification initiation, assuming that cellular dendrites advance continuously from the bottom to the surface. The growth rates along the central axis of Al-5%Mg spot weld are shown as a function of the depth in **Fig. 5**. Without the latent heat, they should become gradually faster from 0.1m/s to more than 10 m/s with approaching to the surface. On the other hand, the growth rate calculated by Mode I considering the latent heat gets faster from about 0.1m/s to 0.5m/s as the interface of dendrite tips approaches to 0.05mm from 0.35mm in depth. Similarly, that of Mode III is about 0.25m/s in the most part. These growth rates are still extremely rapid compared with those in arc welds. The growth rates of cellular dendrite tips are slower by approximately 2 - 10 times in the region from the bottom to the surface due to the effect of the latent heat liberation.

The effect of the latent heat on cooling rate and temperature gradient was also calculated. These results are shown in **Figs. 6** and **7**. The cooling rates become about 2 - 4 times slower and the temperature gradients are reduced in around half due to the effect of the latent heat evolution.

The solid fraction at each depth was obtained as a function of time. The results showing the effect of latent heat and the difference between Mode I and III are indicated in **Fig. 8** (a) and (b), respectively. It is apparent that the solidification can be delayed by the latent heat release. It is interpreted that the liquid (of a small amount) is retained at the bottom even when the cellular dendrite tips advance up to the 0.1mm depth. Under the Mode III condition, the solid fraction increases at almost constant speed. Assuming that the

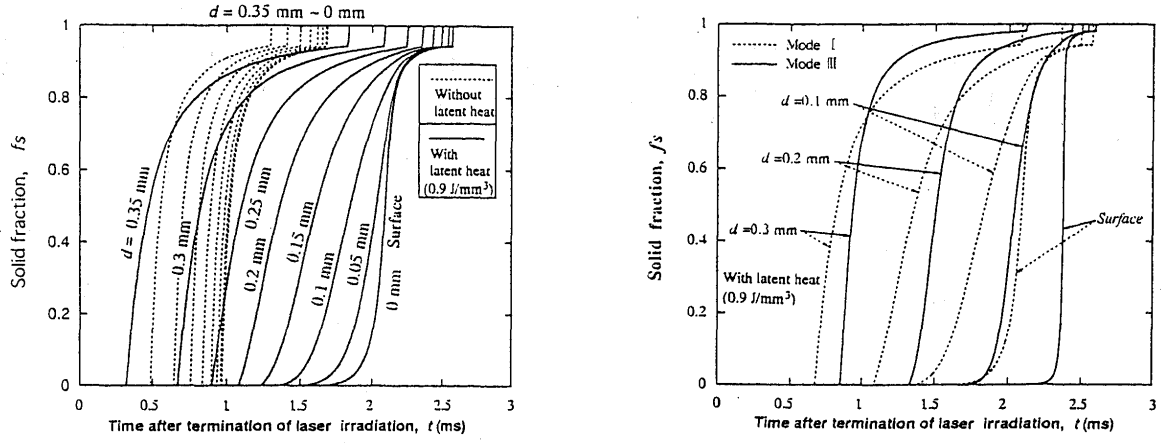

Fig. 8 Variation in solid fraction at each depth as a function of time, showing effect of latent heat (a) and difference between Mode I and III (b) on solid ratio along central axis of weld fusion zone

primary arm spacing is about 1 μ m[14], the lateral (thickening) growth rates are estimated to be about 1 and 2 mm/s for the models of Mode I and Mode III, respectively. This signifies that the thickening rates of cellular dendrite trunks are about 100-200 times slower than the advancing rates of their tips. This result suggests that the interdendritic solute distribution under rapid solidification conditions should be obtained by taking these growth rates into account.

3.4 Actual melting and solidification behaviour and cracking tendency in laser spot welding

The effects of pulsed laser power shapes were investigated by performing laser welding experiment and calculation of the model in order to reveal whether it would be feasible to suppress rapid solidification of cellular dendrite tips, to narrow mushy zones and to reduce or prevent cracking with temporally controlled pulse shapes.

Almost rectangular shapes with and without the addition of tailing power (shown in the upper part of Fig. 11) were utilized. Surfaces and cross sections of heat-conduction type spot welds in A5083 alloy produced under the respective pulse shape conditions are demonstrated in **Fig. 9**. It is apparent that the controlled pulse shape with the tailing power added is beneficial to the reduction in cracking. It was also confirmed that solidification cracking

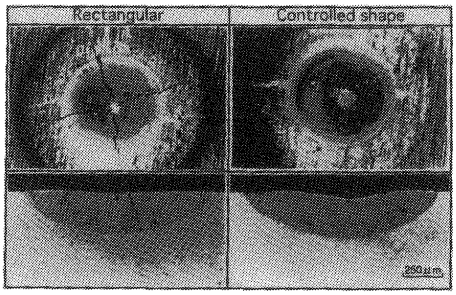

Fig. 9 Surfaces and cross sections of conduction mode spot welds in A5083 alloy produced with laser in rectangular pulse shapes with and without controlled tailing power.

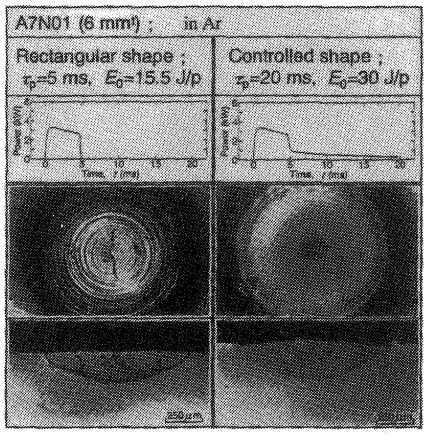

Fig. 10 Surface and cross sections of conduction mode spot welds in A7N01 alloy produced with laser in rectangular pulse shapes with and without controlled tailing power

in A7N01 spot welds could be completely prevented by using such a pulse shape as shown in **Fig. 10**. The reduction or prevention of

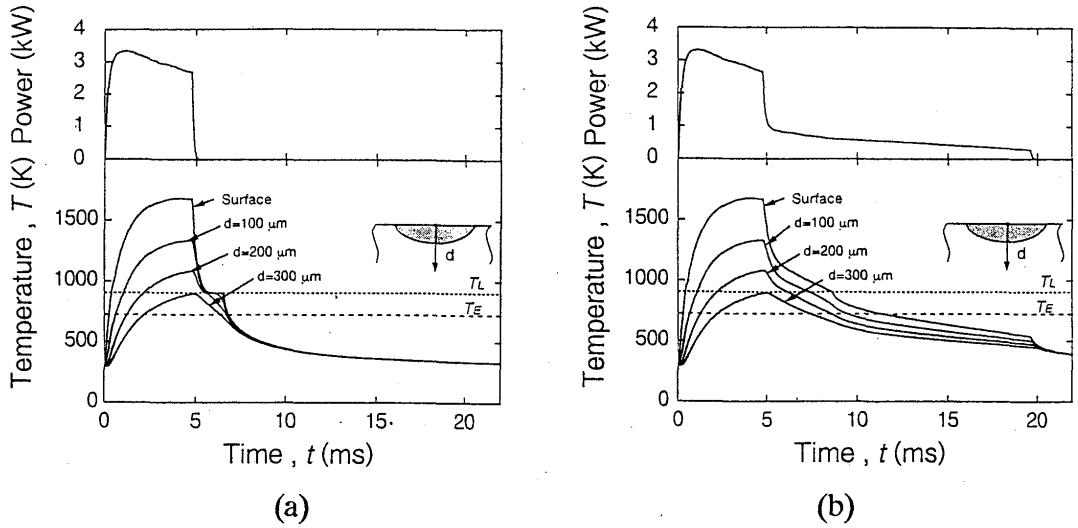

Fig. 11 Output power shapes measured, and calculated temperature histories at various depths in the case of rectangular pulse (a) and pulse with tailing power (b)

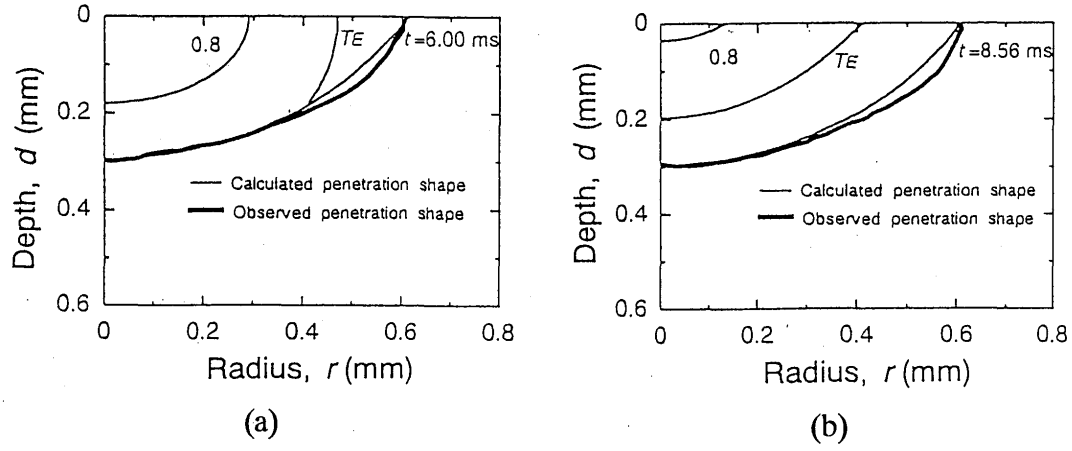

Fig. 12 Comparison between observed and calculated spot weld fusion zones of pulsed laser-welded A5083 alloy, and isothermal temperature distribution when top surface begins to solidify as cellular dendrites in the case of rectangular pulse (a) and pulse with taling power (b)

cracking may be reasonably attributed to a narrower mushy zone, which will be deduced by analyzing melting and solidification behaviour with the present model as follows.

Measured pulse shapes of laser power, calculated temperature histories, variation in solid fraction and isothermal temperature distribution in Al-Mg alloy are compared between two shapes in **Figs. 11** and **12**. It is clearly understood that the tailing power retards cooling at respective depths according to the phenomenon that the solidification occurs gradually from the bottom. When a central surface part begins to solidify, the liquid is present at the bottom in the case of rectangular pulse shape, while the peripheral part of melted zone has completed solidifying to narrow the mushy zone in the case of controlled pulse shape with tailing power.

From the above results, it is understood that an adequate tailing power can retard cooling on account of gradual solidification from the periphery of a laser spot weld and produce narrower mushy zone during solidification. Such pulse shapes for controlled solidification lead to the decrease in cracking sensitivity.

4. Conclusions

A two-dimensional heat-conduction and solidification model considering microsegregation and latent heat was proposed to determine their effects on rapid solidification behaviour and parameters in a laser spot weld. A calculation result demonstrates that a molten pool grows larger in the relatively flat geometry from the surface during melting, while it becomes smaller in the half-round shape during solidification. It is confirmed that cooling is remarkably retarded owing to the latent heat evolution during solidification. The degree of such retardation becomes greater in the region closer to surface. Cooling rates and growth velocities of dendrite tips are slowed down due to the latent heat release. Similarly, temperature gradients are smaller to a slight extent. It is also found in the case of rectangular laser pulse shape that the residual liquid is present along grain boundaries in a wide range of solidifying pool, i.e., a wide mushy zone is formed, resulting in a greater susceptibility to solidification cracking. This is attributed by the fact that the growth rates of dendrite tip in axial and radial directions are greatly different, i.e., 100-200 to 1, which means that the thin film of liquid is retained at the dendrite boundaries in relatively long distance and thus is not resistant to the strain perpendicular to dendrite growth direction. The model could be satisfactorily utilized to reduce solidification cracking in a laser spot weld of crack sensitive alloys.

Acknowledgements

The authors wish to thank Mr. A. Furumoto and Mr. H. Ikeda, the former graduates of Osaka University, for their assistance in the experiments. The authors would also like to appreciate Dr. M. Gremaud, the former visiting researcher of Osaka University, for his valuable discussion and help regarding numerical calculation of microsegregation during rapid solidification.

References

1. A. Matsunawa, S. Katayama, H. Muraki and H. Simidzu: Proc. INALCO '92, Berlin, March 1992, 10.4.1-10.4.10.
2. S. Katayama, S. Kohsaka, M. Mizutani, K. Nishizawa and A. Matsunawa: Proc. ICALEO '93, Nov. 1993, Laser Inastitute of America, 487-497.
3. W.F. Savage: Welding in the World, 1980, **18**, (5/6), 89-104.
4. S.A. David and J.M. Vitek: International Materials Reviews, 1989, **34**, (5), 213-245.
5. I. Ohnaka: Computer Introduction to Heat Transfer and Solidification Analysis - Application to Casting Process, 1985, Maruzen Publishing Co. (in Japanese).
6. M.C. Flemings: Solidification Processing, 1974, New York, McGraw-Hill.
7. W. Kurz and D.J. Fisher: Fundamentals of Solidification, Third Edition, 1989, Trans Tech Publications.
8. R. Trivedi, J. Lipton and W. Kurz: Acta metall., 1987, **35**, (4), 965-970.
9. W.J. Boettinger and S.R. Coriell: Science and Technology of Undercooled Melt - Rapid Solidification Materials and Technologies-, 81-108; 1986, Martinus Nijhoff Publishers.
10. W.J. Boettinger, S.R. Coriell and R. Trivedi: Proc. 45h Conf. on Rapid Solidification Processing, Principles and Technologies, 1987, Santa Barbara, USA.
11. M.J. Aziz: J. Appl. Phys., 1982, **53**, (2), 1158-1168.
12. W. Kurz, B. Giovanola and R. Trivedi: Acta Metall. 1986, **34**, (5), 823-830.
13. M. Rappaz, S.A. Savage, J.M. Vitek and L.A. Boatner: Metallurgical Trans. A, 1990, **21A**, 1767-1782.
14. S. Katayama, H. Muraki, H. Simidzu and A. Matsunawa: Proc. ICALEO '91, 1991, LIA, 352-361.
15. S. Katayama, M. Mizutani, H. Shimidzu and A. Matsunawa: Proc. LAMP'92, 1992, High Temperature Society of Japan, 361-366.
16. S. Katayama, M. Mizutani and A. Matsunawa: Science and Technology of Welding and Joining, 1996, **1**, (1), The Institute of Materials (at Printer)